Estimating Annual Temperate Rain Attenuation Distributions at 20/40 GHz With a High-Resolution Numerical Weather Prediction Model

Laurent Quibus, Valentin Le Mire, Julien Queyrel, Xavier Boulanger, Laurent Castanet, Laurent Féral

Estimating Annual Temperate Rain Attenuation Distributions at 20/40 GHz with a High Resolution Numerical Weather Prediction Model

Laurent Quibus, Valentin Le Mire, Julien Queyrel, Xavier Boulanger, Laurent Castanet and Laurent Féral

***Abstract*—Earth-space communications are to make use of higher frequencies, at and above 20 GHz, to offer new services and increased data rates. A consequence is a strong attenuation of the carrier waves by the troposphere, particularly during rain events. The statistical characterization of the rain attenuation on high frequency channels is thus paramount to their link budget. Traditionally this knowledge is obtained via long-term ground measurements of spaceborne beacon signals. Here, simulated results based on Numerical Weather Prediction models are considered as an alternative. A comparison is given based on two years of beacon data at 20 and 40 GHz in Toulouse (France). Four parametrizations of the WRF model's microphysics are tested: the best performances are achieved with the NSSL-2 moment scheme.**

***Index Terms*—Numerical Weather Prediction, propagation measurements, radio wave propagation, rain attenuation, temperate climate, tropospheric propagation**

I. Introduction

THE growth of satellite communications leads to higher radio-frequencies, so as to achieve higher data rates, and also because the lower frequency bands are saturated. In a typical case, the links between satellite and users would operate in Ka band (20/30 GHz), while the links between the satellite and the network gateways would use the Q/V band (40/50 GHz) or the W band (70/80 GHz) [1], [2].

Unfortunately, high frequency radio-signals are even more strongly impaired within the troposphere. Most notably, the presence of rain on the link attenuates the signal to levels immitigable by power control, so that other techniques must be designed to maintain a high availability ($\gg$ 99.9%) [3]. In that context, it is essential to have a sufficient statistical knowledge of the occurrence of rain attenuation on representative links.

Rain attenuation measurements are obtained thanks to Earth-space propagation experiments, which combine a satellite beacon payload and receiving stations on the ground. The propagation campaigns carried out with ITALSAT (18.7, 39.6, and 49.5 GHz) [4] and ALPHASAT (19.7 and 39.4 GHz) [5] satellites are particularly noteworthy. Most long-term results have been obtained with geosynchronous satellites in temperate zones, though there are recent campaigns for other scenarios [6]-[9]. Long-term means here several years, ideally five to ten, to account for the inter-annual variability of rain [10], [11]. This makes propagation experiments significant investments in time and resources, which cannot easily be extended to any number of sites or frequencies. There is therefore an interest for approaches allowing similar information to be derived for a larger sample of locations and frequencies.

Numerical Weather Prediction (NWP) models are in principle ideal tools to reproduce past states of the troposphere, including precipitations when initiated by reanalysis databases such as ERA Interim [12]. Nowadays global archives such as ERA5 are available to the public at increasingly high resolutions in space (~30 km horizontally) and time (every hour). However, to model the rain attenuation, a downscaling (to ~1-5 km) and an output stored at shorter intervals (~5 min) are needed. Methods to simulate the tropospheric attenuation with high resolution NWP results were developed by [13] and by [14], [15]. A similar approach was taken in the context of Deep-Space missions [16]. Other relevant works include [17]-[20]. It was generally observed that simulated rain attenuation time series correlate poorly with measurements (10-30%). However, acceptable agreements (within 1-5 dB) have been reported for the corresponding rain attenuation Complementary Cumulative Distribution Functions (CCDFs) [12], [15].

In this work, NWP simulations with the Weather Research and Forecasting (WRF-ARW) model serve as the basis for the statistical study of rain attenuation over a period of two years. Reference beacon measurements in Toulouse (France) are available at 20.2 GHz and 39.4 GHz. An objective of this comparison is to test several parametrizations of the meteorological model water microphysics to conclude on an optimal candidate. Preliminary results were given in [21] for three months, to help screen for promising parametrizations.

This work was supported by the Office National d'Études et de Recherches Aérospatiales (ONERA) and by the Centre National d'Études Spatiales (CNES). *(Corresponding author: Laurent Castanet.)*

J. Queyrel and L Castanet are with ONERA, 31055 Toulouse, France (e-mail: julien.queyrel@onera.fr; laurent.castanet@onera.fr).

X. Boulanger is with CNES, 31401 Toulouse, France (e-mail: xavier.boulanger@cnes.fr).

L. Quibus was with ONERA, then CNES. He is now with the Académie Militaire de Saint-Cyr Coëtquidan, 56381 Guer, France (e-mail: laurent.quibus@st-cyr.terre-net.defense.gouv.fr).

V. Le Mire was with ONERA. He is now with Airbus, 31300 Toulouse, France, (e-mail: valentin.le-mire@airbus.com).

L. Féral is with the Laboratoire d'Aérologie, Observatoire Midi-Pyrénées, 31400, Toulouse, France (e-mail: laurent.feral@aero.obs-mip.fr)

Color versions of one or more of the figures in this article are available online at http://ieeexplore.ieee.org

The letter starts in Section II with a description of the beacon and NWP data in use, as well as the conversion and comparison methods. The discussion of the results in terms of CCDFs takes then place in Section III, and Section IV concludes the letter.

II. Data and Methodology

A. *Propagation Experiment in Toulouse*

The ground station under consideration is located in Toulouse (43.57°N, 1.47°E). The French city has a temperate climate with influences from the Atlantic Ocean and the Mediterranean Sea. Beacon measurements are available from two geosynchronous satellites: at 20.2 GHz, from ASTRA-3B (longitude 23.5°E), and at 39.4 GHz, from ALPHASAT (longitude 25°E). The mean elevation and azimuth are almost identical for both links at ~35° and ~150° respectively. For this study, a two-year period of concurrent measurements is chosen from 2015/07 to 2017/06.

The data product of reference in the study of the rain attenuation is the attenuation in excess A_{exc} (dB). The procedure to extract A_{exc} from the beacon measurements is extensively described in [22]-[23].

B. *Numerical Weather Prediction Model*

The Weather Research and Forecasting (WRF) model 4.0.3 and its Advanced Research WRF (ARW) core constitute a regional NWP model [24]. This model is capable to produce atmospheric forecasts over a limited area, at resolutions down to a few kilometers horizontally and a few minutes in time, being given suitable input from a global model. In this work, the input data comes from the ERA5 re-analysis database on pressure and surface levels (every 1 h, 0.25° horizontally) [25].

To cover the period of interest, a simulation is produced for individual days with a spin-up period of 12 h. Each simulation takes place within two consecutive 100 × 100 Lambert Conformal Conic domains centered on Toulouse, the outer domain d01 with a resolution of 6 km, and the inner domain d02 with a resolution of 2 km (see Fig. 1). The post-processing into rain attenuation is performed on the inner domain, for which a datacube of atmosphere is stored every 5 min.

WRF has many configuration settings and options [24]. Here the configuration is the same as described in [21], that is:

- 37 verticals levels.
- hydrostatic solver for d01, non-hydrostatic solver for d02.
- fixed time steps, 36 s for d01 and 12 s for d02.
- no cumulus scheme for either d01 or d02.
- Rapid Radiation Transfer Model for General Circulation Models (RRTMG) radiation scheme, every 6 min for d01 and every 2 min for d02.
- thermal diffusion only land-surface scheme.
- 5th Mesoscale Model (MM5) surface layer and Yonsei University planetary boundary layer schemes, every 5 min.
- Rayleigh implicit gravity-wave damping layer (0.2 s^{-1}).
- spectral analysis nudging (default, above 10th level).

Based on the observations made in [21], a subset of four promising microphysics parametrizations has been selected (see more explanations at Section II-C):

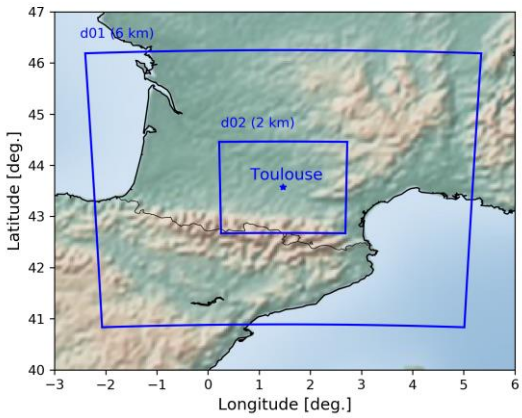

Fig. 1. WRF simulation domains' horizontal extents around Toulouse: outer domains d01 (6 km) and inner domain d02 (2 km)

- single-moment: Lin and WSM6.
- double-moment: WDM6 and NSSL [26].

As a last practical point, to limit the computation time, simulations are restricted to rainy days [27]. The selected days are considered as rainy if at any time the hourly ERA5 rain rate exceeds a given threshold for the pixel nearest to Toulouse. The threshold is obtained by computing the monthly CCDF of the ERA5 rain rate and taking the exceeded rain rate for 20% of the time. In any case the threshold is also capped at 1 mm h^{-1}. The gain in computing time is substantial (~40-45%). When tested with the full year 2016, this restriction incurs an RMS error of only ~0.01 dB on the rain attenuation CCDF.

C. *Rain Attenuation Model*

In order to simulate the rain attenuation using NWP datasets, a method accounting for the full tridimensional information was proposed in [14]. It first consists in computing, at every point on the grid, the specific rain attenuation γ_R (dB/km) according to the Mie scattering theory [28]

$$\gamma_R = \gamma_{R,0} \int_0^\infty \sigma_{ext}(f,T,D) n_R(D) dD \qquad (1)$$

with $\gamma_{R,0} = 4.343$ dB m/km, the frequency f (GHz), the air temperature T (K), and involving the extinction cross-section σ_{ext} (m^2) as well as the rain drop size distribution n_R (m^{-1} m^{-3}), both of which depend furthermore on the drop diameter D (m).

The Mie solution for σ_{ext} is considered here as in [14], taking the liquid water refractivity model from Ray [29]. The rain drop size distribution n_R is, importantly, chosen to be consistent with the assumptions of the NWP model (here: WRF). It means that n_R is a gamma distribution such as

$$n_R(D) = N_R \frac{\Lambda}{\Gamma(\mu+1)} (\Lambda D)^\mu \exp(-\Lambda D) \qquad (2)$$

with Γ the gamma function, with μ and Λ (m^{-1}) the distribution parameters, and where N_R (m^{-3}) is the number of drops per unit volume (i.e. the normalization factor). In (2) the value of μ is fixed, whereas (N_R, Λ) vary with the atmospheric conditions. For a double-moment microphysics, both N_R and Λ vary independently. For a single-moment microphysics, they are related and (2) simplifies into

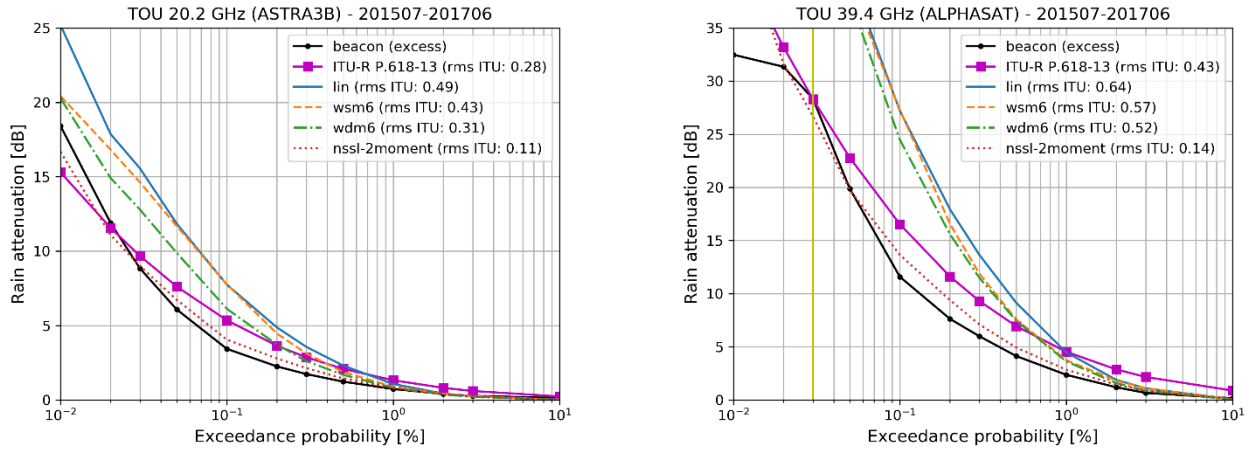

(a) (b)

Fig. 2. Complementary Cumulative Distribution Functions (CCDFs) of the rain attenuation in Toulouse during the two-year period from 2015/07 to 2017/06. The beacon measurements are compared to the ITU-R reference model and to the NWP-based results. (a) 20.2 GHz, and (b) 39.4 GHz.

$$n_R(D) = N_{R,0} D^{\mu} \exp(-\Lambda D) \quad (3)$$

with $N_{R,0}$ ($\mathrm{m}^{-(3+\mu)}$) being a characteristic fixed value.

Either one or two output variables are necessary to reconstruct the distribution. The first is the rain mass mixing ratio q_R (kg kg^{-1}), *i.e.* the mass of rain water per unit mass of dry air, the second is the number of rain drops mixing ratio q_{N_R}(kg^{-1}), i.e. the number of rain drops per unit mass of dry air. The details on how to use these variables to get to Λ or (N_R, Λ), for a single or double-moment distribution respectively, are laid out in [12], [14] and [27] respectively.

In practice, the following distributions are considered here:

- the single-moment schemes Lin and WSM6 use $\mu = 0$ and $N_{R,0} = 8 \times 10^{-6}$ m^{-1} m^{-3}. Their distribution is thus exponential, and also the Marshall-Palmer distribution.
- the double-moment scheme NSSL assumes $\mu = 0$. Its distribution is also exponential, but $N_{R,0}$ is not a constant.
- the double-moment scheme WDM6 assumes $\mu = 1$. Its distribution is thus a less trivial case of gamma distribution for which $N_{R,0}$ is also not a constant.

It is worth remarking there is little variety in the types of distributions being considered. This is a consequence of working with the subset of microphysics offered by WRF [24], whereas more options exist generally [30]. Generalized gamma distributions have notably been shown to lead to an improved modelling of measured drop size distributions [31]. Another well-known point to keep in mind is that it is not accurate to describe larger rain drops as spherical [32], and Mie theory is then often supplanted by the T-matrix method [33]. Staying consistent with the assumptions of the NWP model is however a central point of this work, hence the drops are considered as spherical for electromagnetic computations as well.

Be that as it may, once γ_R (dB/km) has been retrieved from (1), obtaining the rain attenuation A_R (dB) along a certain path within the NWP domain is a matter of interpolating and integrating γ_R along that path. The simulated attenuation time series have then a resolution of 5 min, like the NWP data.

D. *Distributions and Comparison Metric*

At the cornerstone of the investigation, the Complementary Cumulative Distribution Functions (CCDFs) of the measured and simulated attenuations are produced from their respective time series. As another point of comparison, the long-term annual CCDFs predicted with Recommendation ITU-R. P.618-13 [34] are considered too.

In order to compare the parametrizations, the standard adimensional ITU-R rain attenuation error metric [35] is computed for each of the CCDFs, with the beacon excess attenuation CCDF given as the reference.

The range of probabilities being studied is from 0.01% to 10% for annual CCDFs. For lower exceedance probabilities, the number of NWP output samples, every 5 min, is too small to give meaningful results. The set of probabilities selected to compute the error are those from [35], that is: 0.01%, 0.02%, 0.03%, 0.05%, 0.1%, 0.2%, 0.3%, 0.5%, 1%, 2%, 3%, and 10%.

Further restrictions are imposed to improve the quality and fairness of the comparisons. First, at high percentages of time, the measured attenuation must exceed 0.5 dB before the point is included into the error: this is to account for the limitation of the excess attenuation processing, e.g. the inclusion of residual cloud attenuation at lower attenuation values. Second, if a breakpoint is observed in the measured CCDF, the values at lower probabilities are not considered: this is to account for the impact of the limited dynamic range of the measurement system, in other terms the "saturation plateau" is not considered in the testing activity.

III. Comparison of the Measured and Simulated CCDFs

A. *Ka Band (20.2 GHz)*

Fig. 2a shows the measured and simulated CCDFs for Toulouse at 20.2 GHz for the two-year period. The curves are for the beacon (excess) measurements (in black, solid line with dot markers), the reference Recommendation ITU-R P.618-13 model (in magenta, solid line with square markers), and the four NWP microphysics parametrizations under study: Lin (blue, solid line), WSM6 (orange, dashed line), WDM6 (green,

dashed dotted line), and NSSL (red, dotted line). The ITU-R RMS error metrics are provided within the legend for each model, as compared to the beacon (excess) reference curve.

It is observed that the best overall agreement exists between the measured CCDF and the NSSL CCDF, which is corroborated by the lowest value of the ITU-R metric (0.11). Down to roughly 0.03% of the time, NSSL follows closely the beacon with a slight overestimation not exceeding ~1 dB. Below 0.03%, NSSL is overtaken by the beacon measurements but remains within a couple of dBs from it.

The second best performing model is actually the rain attenuation model of Recommendation ITU-R P.618-13, with an ITU-R error of 0.28. This model behaves worse than NSSL, with a noticeably stronger overestimation of the beacon above 0.03% of the time, with for example a difference of 2 dB with respect to a predicted 5 dB excess attenuation at 0.1 %.

Even more, the other NWP-based CCDFs give worse results in terms of ITU-R error, with respectively 0.31 for WDM6, 0.43 for WSM6, and 0.49 for Lin. For high percentages of the time, they initially outperform the ITU-R model by having a lower overestimation of the beacon, but this overestimation quickly gets worse below 0.5% of the time. The strength of the overestimation follows the same order as the error metric, it is strongest in Lin, then WSM6, then WDM6. In that regard, the double-moment schemes (WDM6, NSSL) perform better than the single-moment schemes (Lin, WSM6).

B. *Q Band (39.4 GHz)*

Fig. 2b shows the measured and simulated CCDFs for Toulouse at 39.4 GHz. The curves are colored and labelled as for the 20.2 GHz case. The ITU-R error metrics are provided in the legend as well. Note that there is a breakpoint in the beacon CCDF slope around 0.03% of the time, which means that lower exceedance probabilities are excluded from the error metric.

Most of the observations made at 20.2 GHz are present at 39.4 GHz, which is an important point to select a best performing parametrization, since the results at a single frequency are not guaranteed to scale favorably with frequency.

Again, the NSSL CCDF has the lowest ITU-R error (0.14) and outperforms clearly the other models. The overestimation of the beacon CCDF lasts till 0.05%, reaching ~2-3 dB at most. The behavior of the NSSL CCDF past the beacon CCDF breakpoint is also similar to the one at 20.2 GHz.

The ITU-R P.618 CCDF has the second best performance (0.43) still, and behaves significantly worse than NSSL, with a noticeably stronger overestimation of the beacon above 0.03% of the time (5 dB at 0.1 %).

The other NWP-based models show again poorer performances, in the same order as before: WDM6 (0.52), WSM5 (0.57), Lin (0.64), especially for time percentages lower than 1 %. For time percentages higher than 1 %, they performs better than Recommendation ITU-R P.618-13. If the overestimation could still look quite reasonable at 20.2 GHz, here it can exceeds 10 dB however.

IV. Conclusion

This letter compared annual CCDFs of the rain attenuation simulated with the WRF high resolution weather forecast model coupled with a physical propagation model, and the one predicted with the Recommendation ITU-R P.618-13, to the experimentally derived one. The comparison concerned Toulouse, over a two-year period at 20.2 and 39.4 GHz.

It was found that, everything else being equal, the choice of the NSSL-2-moment scheme provides the best performances, while the other microphysics selected give worse results. The NSSL scheme was developed to study thunderstorms, first in the vicinity of its namesake the National Severe Storms Laboratory in Norman, Oklahoma [26]. Though temperature extremes and precipitation amounts are significantly higher in Norman than in Toulouse, both locations have a temperate humid with hot summers (Cfa) Köppen classification. Considering also that thunderstorms are the main source of high attenuation events in a temperate climate, this gives some clues as to why NSSL performs well.

The main conclusion of this work is that testing several microphysics is a worthwhile endeavor to find a better candidate most capable to reproduce measured rain attenuation statistics. The soundness of the analysis is here reinforced by the stability of the results obtained at two frequencies. There is an interest in using more complex, double-moment, microphysics and properly accounting for their rain drop size distributions, even more with increasing frequency. It is not expected however that one microphysics would always yield the best result for any other sites even in temperate climates.

As often, the confidence in the results would improve with a longer measurement period, more in-line with the interannual variability of rain, and by including multiple sites.

References

[1] R. De Gaudenzi, P. Angeletti, D. Petrolati, and E. Re, “Future technologies for very high throughput satellite systems,” *Int. J. Satell. Commun. Networking*, vol. 38, no. 2, Mar. 2019.

[2] L. Luini, R. Nebuloni, and C. Riva, “Ka-to-W Band EM wave propagation: tropospheric effects and countermeasures,” in *Wave Propagation Concepts for Near-Future Telecommunication Systems*. IntechOpen, 2017.

[3] A. Panagopoulos, “Propagation Phenomena and Modeling for Fixed Satellite Systems: Evaluation of Fade Mitigation Techniques,” in *Radio wave propagation modeling for Earth-space systems*. CRC Press, 2016.

[4] C. Riva. “Seasonal and diurnal variations of total attenuation measured with the ITALSAT satellite at Spino d’Adda at 18.7, 39.6 and 49.5 GHz,” *Int. J. Satell. Commun. Networking*, vol. 22, no. 4, Jul. 2004.

[5] C. Riva and A. Martellucci, “Preface to the special issue on the Alphasat Aldo Paraboni propagation experiment,” *Int. J. Satell. Commun. Networking*, vol. 37, no. 5, May 2019.

[6] T. Tjelta, M. Rytir, L.E. Bråten P.A. Grotthing, M. Cheffena, and J.E. Håkegård, “Results of Ka Band Campaign for the Characterisation of Propagation Conditions for SatCom Systems at High Latitudes,” in *Proc. 11th Eur. Conf. Antennas Propag. (EuCAP)*, Paris, FR, 2017.

[7] X. Boulanger, B. Benammar, and L. Castanet, “Propagation Experiment at Ka-Band in French Guiana: First Year of Measurements,” *IEEE Antennas and Wireless Propag. Lett.*, vol. 18, no. 2, Feb. 2019.

[8] A.M. Marziani, F. Consalvi, A. Rocha, S. Mota, L. Luini, C. Riva, and F.S. Marzano, “MEO Satellite Ka-Band Receiving Stations for Tropospheric Propagation Impairment Analysis: Design, Architecture and Preliminary Measurements,” in *Proc. 15th Eur. Conf. Antennas Propag. (EuCAP)*, Dusseldorf, DE, 2021.

[9] F. Cuervo, A. Martín-Polegre, F. Las-Heras, D. Vanhoenacker-Janvier, J. Flávio, and M. Schmidt, “Preparation of a Cubesat LEO radio wave propagation campaign at Q and W bands,” *Int. J. Satell. Commun. Networking*, vol. 40, no. 1, Jan. 2022.

[10] N. Jeannin, X. Boulanger, L. Féral, L. Castanet, and F. Lacoste, “Inter-annual variability, risk and confidence intervals associated with propagation statistics. Part I: theory of estimation,” *Int. J. Satell. Commun. Networking*, vol. 32, no. 5, Sep. 2014.

[11] X. Boulanger, N. Jeannin, L. Féral, L. Castanet, F. Lacoste, and F. Carvalho, “Inter-annual variability, risk and confidence intervals associated with propagation statistics. Part II: parametrization and applications,” *Int. J. Satell. Commun. Networking*, vol. 32, no. 5, Sep. 2014.

[12] L. Castanet, V. Le Mire, J. Queyrel, X. Boulanger, and L. Féral, "Potentialities of a mesoscale meteorological model to reproduce experimental statistics of rain attenuation on Earth-space paths”, *Int. J. Antennas Propag., Oct.* 2022.

[13] D.D. Hodges, R.J. Watson, and G. Wyman, “An Attenuation Time Series Model for Propagation Forecasting,” *IEEE Trans. Antennas Propag.*, vol. 54, no. 6, Jun. 2006.

[14] M. Outeiral García, N. Jeannin, L. Féral, and L. Castanet, “Use of WRF to Characterize Propagation Effects in the Troposphere,” in *Proc. 7th Eur. Conf. Antennas Propag. (EuCAP)*, Göteborg, SE, 2013.

[15] N. Jeannin *et al.* “Atmospheric Channel Simulator for the Simulation of Propagation Impairments for Ka Band Data Downlink,” in *Proc. 8th Eur. Conf. Antennas Propag. (EuCAP)*, The Hague, NL, 2014.

[16] M. Biscarini, A. Vittimberga, K. De Sanctis,S. Di Fabio, M. Montagna, L. Milani, Y. Tsuda, and F.S. Marzano, “Optimal Stochastic Prediction and Verification of Signal-to-Noise Ratio and Data Rata Ka-Band Spaceborne Telemetry Using Weather Forecasts,” *IEEE Trans. Antennas Propag.*, vol. 69, no. 2, Feb. 2021.

[17] G. Fayon, L. Féral, L. Castanet, N. Jeannin, and X. Boulanger, “Use of WRF to Generate Site Diversity Statistic in South of France,” in *Proc. 32nd URSI GASS*, Montréal, CA, 2017.

[18] F. Cuervo et *al*. “Short Term Satellite Channel Characteristics Forecast Using Numerical Weather Prediction Data,” in *Proc. 12th Eur. Conf. Antennas Propag. (EuCAP)*, London, UK, 2018.

[19] K. Grythe, L.E. Bråten, S.S. Rønning, and T. Tjelta, “Predicting near-time satellite signal attenuation at Ka-band using tropospheric weather forecast model,” in *Proc. 12th Eur. Conf. Antennas Propag. (EuCAP)*, London, UK, 2018.

[20] V. Le Mire, X. Boulanger, L. Castanet, B. Bennamar, and L. Féral, “Potentialities of the Numerical Weather Prediction model WRF to produce attenuation statistics in tropical regions,” in *Proc. 14th Eur. Conf. Antennas Propag. (EuCAP)*, Copenhagen, DK, 2020.

[21] L. Quibus, V. Le Mire, J. Queyrel, L. Castanet, and L. Féral, “Rain Attenuation Estimation with the Numerical Weather Prediction Model WRF: Impact of Rain Drop Size Distribution for a Temperate Climate,” in *Proc. 15th Eur. Conf. Antennas Propag. (EuCAP)*, Dusseldorf, DE, 2021.

[22] X. Boulanger, B. Gabard, L. Casadebaig, and L. Castanet. “Four Years of Total Attenuation Statistics of Earth-Space Propagation Experiments at Ka-band in Toulouse,” *IEEE Trans. Antennas Propag.*, vol. 63, no. 5, May 2015.

[23] X. Boulanger and L. Castanet. “Ka and Q band propagation experiments in Toulouse using ASTRA 3B and ALPHASAT satellites,” *Int. J. Satell. Commun. Networking*, vol. 37, no. 5, Sep. 2019.

[24] W.C. Skamarock *et al.*, “A Description of the Advanced Research WRF Version 4,” NCAR, Boulder, CO, Tech. Rep. NCAR/TN-566+STR, Mar. 2019.

[25] H. Hersbach et al., “The ERA5 global reanalysis,” *Quarterly J. Royal Meteorological Society*, vol. 146, no. 730, Jul. 2020.

[26] E.R. Mansell, C.L. Ziegler, and E.C. Bruning. “Simulated Electrification of a Small Thunderstorm with Two-Moment Bulk Microphysics,” *J. Atmos. Sci.*, vol. 67, no. 1, Jan. 2010.

[27] V. Le Mire, “Modélisation de la propagation Terre-Espace en bande Ka dans les zones tropical et équatoriales, ” Ph.D. dissertation, Université de Toulouse, 2021.

[28] H.C. van de Hulst, *Light scattering by small particles*. Dover Publications, 1981.

[29] P.S. Ray, “Broadband Complex Refractive Indices of Ice and Water,” *Applied Optics*, vol. 11, no. 8, Aug. 1972.

[30] A.P. Khain et al., “Representation of microphysical processes in cloud-resolving models: Spectral (bin) microphysics versus bulk parameterization,” *Rev. Geophys.*, vol. 53, no. 2, Jun. 2015.

[31] M. Thurai, V. Bringi, P.N. Gatlin, W.A. Petersen, M.T. Wingo, “Measurements and modelling of the full rain drop size distribution,” *Atmopshere*, vol. 10, no. 1, 2019.

[32] M. Thurai, S. Steger, F. Teschl, M. Schönhuber, and D.B. Wolff, “Rain Drop Shapes and Scattering Calculations: A Case Study Using 2D Video Disdrometer Measurements and Polarimetric Radar Observations at S-band During Hurricane Dorian Rain-Bands,” in *Proc. 15th Eur. Conf. Antennas Propag. (EuCAP)*, Dusseldorf, DE, 2021.

[33] M.I. Mishchenko, G. Videen, V.A. Babenko, N.G. Khlebtsov and T. Wriedt, “T-matrix theory of electromagnetic scattering by particles and its applications: a comprehensive reference database,” J. Quant. Spectrosc. Radiat. Transfer, vol. 88, no. 1, Sep. 2004.

[34] International Telecommunication Union Radiocommunication (ITU-R), “Recommendation ITU-R. P.618-13: Propagation data and prediction methods required for the design of Earth-space telecommunication systems,” Dec. 2017.

[35] International Telecommunication Union Radiocommunication (ITU-R), “Working Party 3M Fascicle on testing variables used for the selection of prediction methods,” Jul. 2016.